ACOUSTICALLY COUPLED WIDEBAND RF FILTERS WITH BANDWIDTH RECONFIGURABLITY USING FERROELECTRIC ALUMINUM SCANDIUM NITRIDE FILM

Sushant Rassay, Faysal Hakim, Mehrdad Ramezani, and Roozbeh Tabrizian
Electrical and Computer Engineering Department, University of Florida, Gainesville, FL, USA

ABSTRACT

This paper reports a 2.3 GHz wideband acoustically coupled filter with large bandwidth reconfigurability realized in ferroelectric aluminum-scandium-nitride ($Al_{0.7}Sc_{0.3}N$) films. Benefiting from large electromechanical coupling of the $Al_{0.7}Sc_{0.3}N$ film, bandwidths ~3-times larger compared to state-of-art AlN acoustically coupled counterparts are achieved Furthermore, for the first time, we are demonstrating the use of the recently discovered ferroelectricity in $Al_{1-x}Sc_xN$ films (x>27%) for large bandwidth tuning of the filter. The acoustically coupled filter architecture provides superior characteristics compared to conventional electrically coupled filters (i.e. lattice, ladder, etc.) including the lithographical bandwidth definition through proper IDT patterning, and realization of the filter within a single / monolithic structure. Here 1µm-thick $Al_{0.7}Sc_{0.3}N$ films are acoustically engineered to implement 2.3 GHz filters with -3dB bandwidths (BW_{-3dB}) over 70-117 MHz are demonstrated with an insertion loss of -6dB (dominated by the routing line resistance). Large tuning of 15 MHz (~15%) is achieved through application of ~60 volts, DC, using a bias-tee. Such high-performance filters enable realization of reconfigurable RF front-end for emerging multi-band wireless systems that require extensive compatibility with a wide variety of communication standards in the forthcoming 5G landscape.

INTRODUCTION

Realization of high-performance RF filters within a monolithic structure has always been intriguing in acoustic device community as it reduces overall foot-print of the filter, eliminates various fabrication, packaging and reliability challenges, and reduces routing parasitics inherent to electrically coupled acoustic filters (such as BAW ladder, lattice, etc.) [1-4]. While the idea of acoustic coupling of two resonance modes within a single structure promises realization of a monolithic filter, achieving comparable performance with electrically coupled counterparts has been challenging. Specifically, acoustically coupled filters suffer from lower bandwidth and larger insertion loss; both of which resulted from partial electrode-coverage inherent to the IDT design of the two-port acoustically coupled filter. These problems, however, can be surpassed through the use of aluminum-scandium-nitride films that are recently gaining large interest due to providing significantly higher electromechanical coupling compared to AlN counterparts. Furthermore, the very recent discovery of the ferroelectric property in $Al_{1-x}Sc_xN$, when Sc-content (i.e. x) exceeds 27%, opens promising opportunities including agile reconfiguration of the filter through tuning polarization and dielectric constant using a DC voltage.

In this work, we demonstrate a high-performance acoustically coupled filter with wide bandwidth reconfigurability implemented in reactively sputtered $Al_{0.7}Sc_{0.3}N$ films. The filters are created by etching semi-trenches in $Al_{0.7}Sc_{0.3}N$ to define a trapezoid acoustic cavity for efficient energy trapping of various extensional bulk acoustic modes that create a bandpass spectral response. Fig. 1 shows the SEM image of the filter. The cross-sectional SEM image shows the semi-trench used to laterally define the filter. Two sets of IDTs, with 10 fingers each and a pitch size of 5µm, are patterned on the top Mo layer to form the input and output ports. The $Al_{0.7}Sc_{0.3}N$ film is etched, using a high-power chlorine-based recipe, to get access to bottom Mo electrode that covers the cavity.

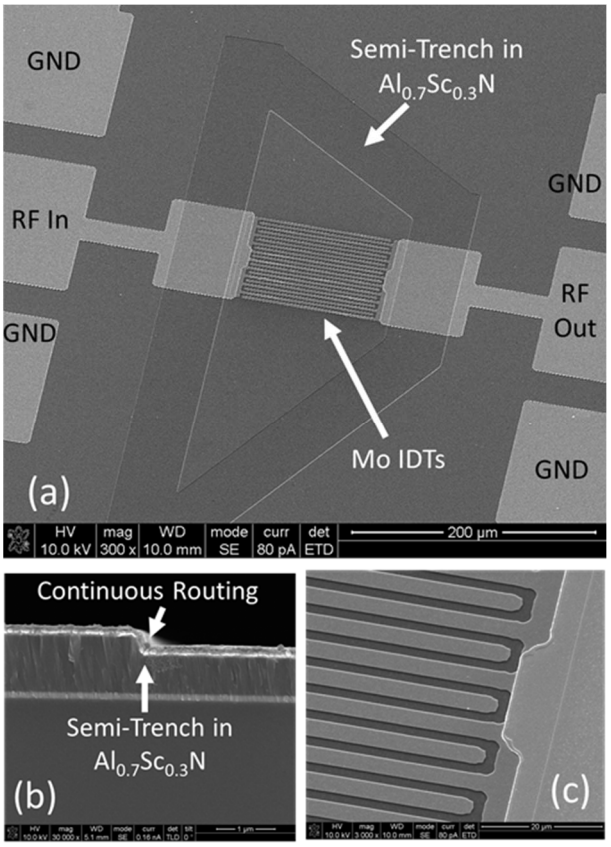

Fig. 1: (a) The SEM image of the acoustically coupled filter implemented in 1µm $Al_{0.7}Sc_{0.3}N$, sandwiched between 100nm Mo electrodes. The IDTs are patterned on the top Mo layer to define the input and output transduction ports of the filter. A trapezoid geometry, with non-parallel edges, are patterned through etching semi-trenches in $Al_{0.7}Sc_{0.3}N$. (b) The cross-sectional SEM showing the electrode coverage over the semi-trench in $Al_{0.7}Sc_{0.3}N$. (c) The zoomed-in IDTs in top Mo layer.

OPERATION CONCEPT AND MODELING

The monolithic filter presented in this work is realized through energy trapping of two types of bulk acoustic vibrations. In the first type (type-I), the S_1 Lamb wave is trapped entirely under the electroded area at the excitation port (i.e. port 1) and is coupled to an evanescent wave in un-electroded regions. Opting for proper thickness of top Mo electrodes, efficient coupling can be achieved to obtain evanescent modes with large wavenumbers. Such an energy trapping results in weak transmission of acoustic energy into neighboring electrodes (i.e. port 2), which translates to sharp notches in the filter response. On the other hand, the second type (type-II) of the modes are symmetric Lamb waves (i.e. S_0, S_1, or S_2) with frequencies defined by the IDT pitch size and propagate across the un-electroded area to efficiently transmit the energy to port 2. COMSOL simulations are used to optimize the electrode thickness and spacing required to form a bandpass filter response, through tailoring the frequency of type-II modes between two type-I modes. Besides the electrode thickness and spacing, the lateral geometry of the filter is optimized to suppress spurious modes outside the passband. Fig. 2 shows the COMSOL-simulated frequency response of the filter for AlN and $Al_{0.7}Sc_{0.3}N$. The simulation is performed by considering a hypothetical case of similar elastic constants for both films, to enable exploration of the effect of material electromechanical coupling coefficient (k_{eff}^2) on the filter performance. While the bandwidth of the acoustically coupled filter should be ideally defined by the IDT thickness and pitch-size, the low electromechanical coupling of AlN results in large pass-band ripples exceeding -3dB. However, this is not the case in $Al_{0.7}Sc_{0.3}N$, thanks to its large k_{eff}^2, resulting in a 3-times increase in 3dB bandwidth (BW_{-3dB}) of the filter compared to AlN counterpart.

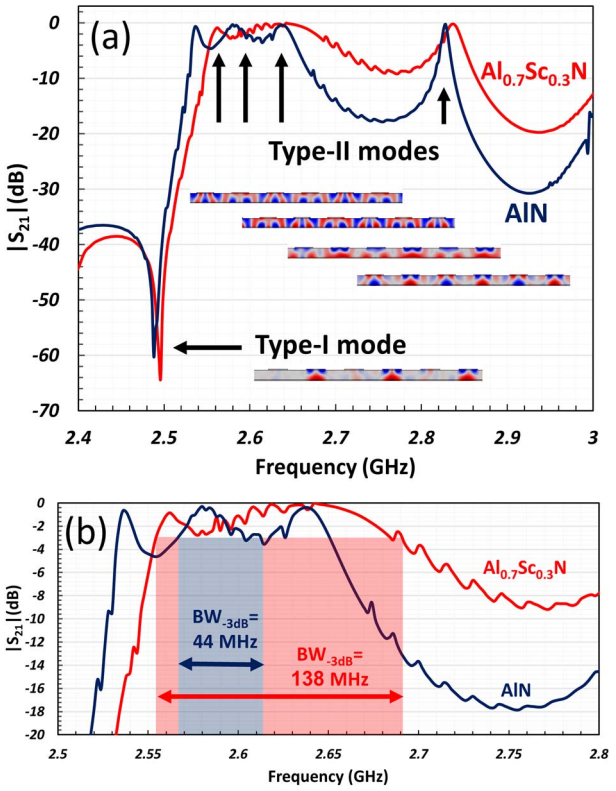

Fig. 2: (a) COMSOL-simulated frequency response of the filter shown in Fig. 1 for AlN and $Al_{0.7}Sc_{0.3}N$ films. No material loss is considered to accurately explore the effect of the electromechanical coupling on bandwidth. The type-I and type-II modes that define the poles and zeros of the filter response are highlighted at their corresponding frequencies. (b) The comparison of the filter passbands, highlighting significant enhancement of the bandwidth in $Al_{0.7}Sc_{0.3}N$ case.

FABRICATION PROCESS

The filter is fabricated in reactively sputtered $Al_{0.7}Sc_{0.3}N$ film, deposited atop of 100nm Mo electrodes and on the top surface of a high resistivity silicon substrate. To ensure suppression of abnormal grains with undesired crystal morphology, a 20nm AlN seed layer is deposited prior to sputtering of the bottom Mo. Fig. 3 (a) shows the

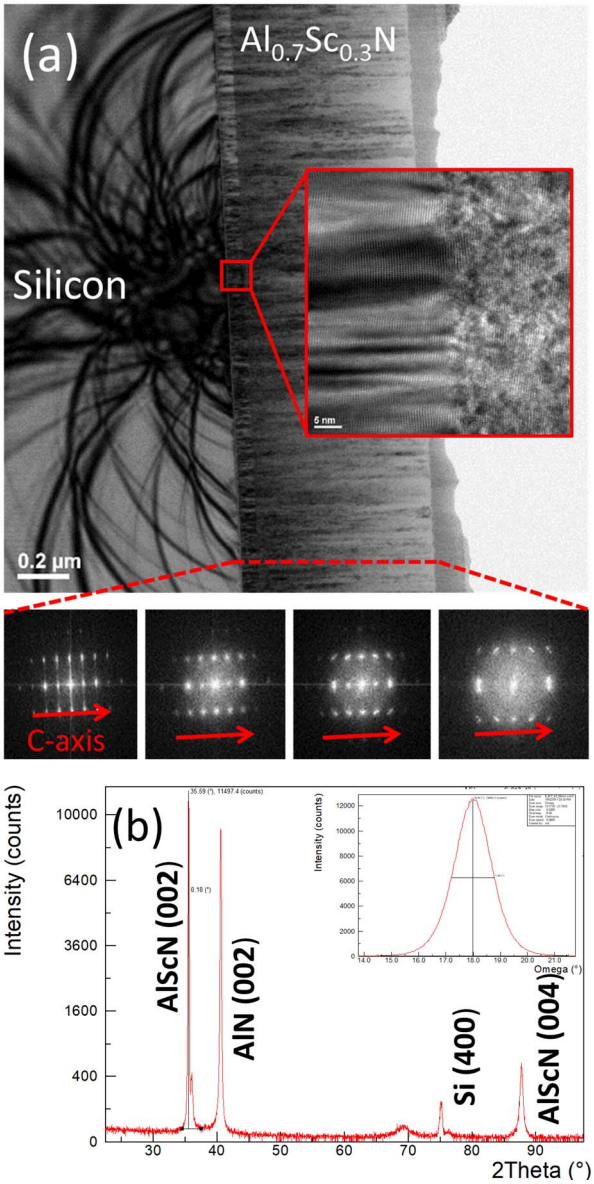

Fig. 3: (a) The cross-sectional high-resolution TEM of the $Al_{0.7}Sc_{0.3}N$ film showing the c-axis texture of the reactively sputtered film. The FFT of diffraction pattern are extracted across the film thickness, highlighting consistently perpendicular c-axis of the film. (b) XRD of the transducer film highlighting an FWHM of 1.56 across

cross-sectional TEM image of the film, highlighting the transducer stack details and $Al_{0.7}Sc_{0.3}N$ film texture. Diffraction patterns are used to verify the direction and consistency of the c-axis across the film thickness. Fig. 3(b) shows the measured XRD of the stack, highlighting an FWHM of 1.56° around (002) $Al_{0.7}Sc_{0.3}N$ peak.

Fig. 4 shows the fabrication process used for implementation of the filter. First, the 1µm $Al_{0.7}Sc_{0.3}N$ is etched to get access to bottom Mo layer that serves as the bottom electrode of the filter. In the next step, semi-trenches are etched, with a depth of 350nm in $Al_{0.7}Sc_{0.3}N$ film to define the lateral geometry of the device. For both $Al_{0.7}Sc_{0.3}N$ etching steps, a high-power Cl_2/H_2 based RIE recipe is used. Etching of AlN films with high Sc content is highly challenging due to formation of undesirable nonvolatile byproducts [5]. In this work we used very large RIE power to enhance physical etching of the film. For this purpose, a thick SiO_2 hard mask is used. Such a hard mask ensures a smooth sidewall of the $Al_{0.7}Sc_{0.3}N$ trenches across the film and enhances energy trapping efficiency. In the next step, a 100nm Mo layer is deposited using lift-off to define the two sets of IDTs (i.e. port 1 and port 2 electrodes) and probing pads. Finally, the device is released by etching Si from the backside via the Bosch process in a DRIE tool.

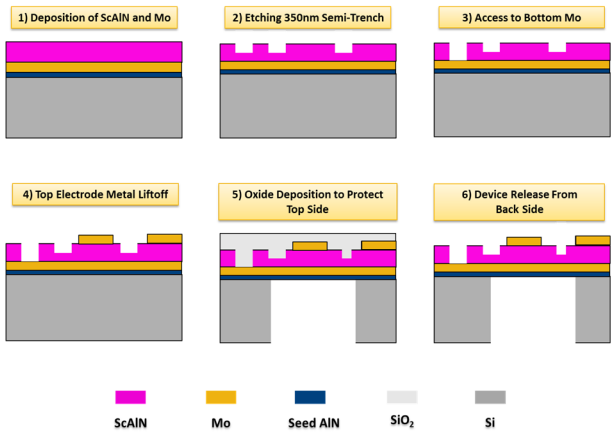

Fig. 4: The fabrication process flow for implementation of acoustically coupled filters in 1µm $Al_{0.7}Sc_{0.3}N$ film. The stack consists of $Al_{0.7}Sc_{0.3}N$ deposited on 100nm Mo film. A seed layer that is used to ensure c-axis textured growth of the $Al_{0.7}Sc_{0.3}N$ film serves as the etch stop during the backside release (i.e. etching Si substrate from backside using Bosch DRIE).

CHARACTERIZATION RESULTS

The fabricated filters are characterized using an N5242A PNA-X Network Analyzer. An input power of -5dB. SOLT calibration across 1-3GHz is used prior to device characterization. Fig. 5 (a) demonstrates the measured filter response and is compared with the lumped-element model. Figure 5 (b) shows the equivalent electrical model of the filter, where the shunt and series resonators correspond to type-I and type-II vibration modes, respectively. An accurate match of the filter response with lumped-element model is shown which illustrates the acoustic operation principle of the filter. A BW_{-3db} of ~70 MHz is measured at f_0 = 2.32 GHz, with an insertion loss

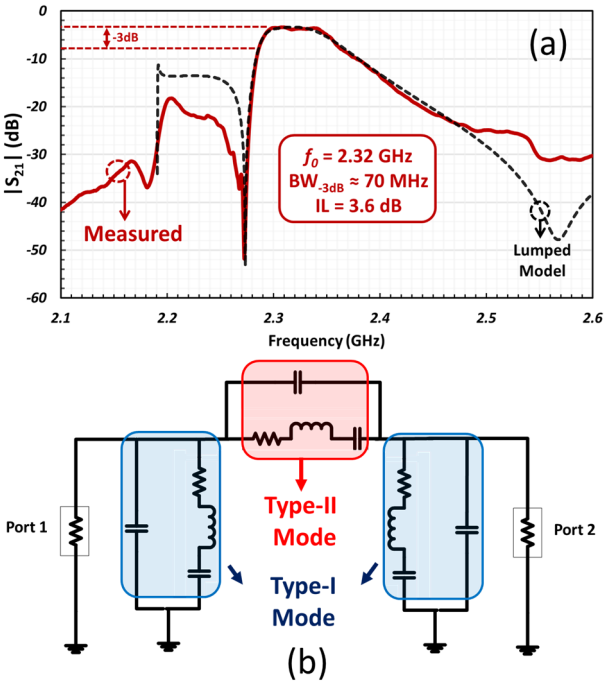

Fig. 5: (a) The measured transmission response (i.e. $|S_{21}|$) of the filter, showing a BW_{-3dB} of ~70 MHz. The measured response is compared with the (b) lumped model suggesting the equivalence with a 1.5-stage ladder architecture (i.e. three resonators), highlighting the promise of the acoustically coupled $Al_{0.7}Sc_{0.3}N$ filter to reduce the foot-print compared to electrically coupled counterparts.

(IL) of -3.6 dB. The filter passband is followed by a sharp roll-off at the lower end. Achieving a similar roll-off at the higher-end requires energy trapping of a secondary type-I mode.

The filters are also explored for their tunability using DC voltages. Ferroelectric switching has been recently demonstrated in $Al_{1-x}Sc_xN$ for Sc-content exceeding 27% [6]. We explore this spontaneous switching polarization in

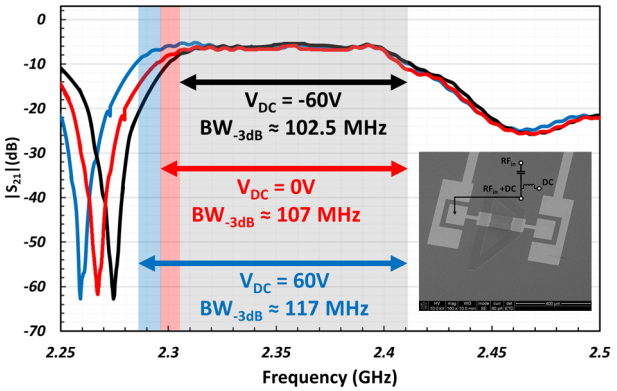

Fig. 6: The bandwidth tunability using DC voltage applied to the input IDT through a bias-tee. The large reconfigurability of the bandwidth is provided by the ferroelectric effect in $Al_{0.7}Sc_{0.3}N$ that facilitates local tuning of the dielectric constant and electromechanical coupling by DC fields through the nonlinear electrostrictive effect. A large bandwidth tunability of ~15MHz (14.7%) is achieved through application of ~60V, DC.

$Al_{0.7}Sc_{0.3}N$ by measuring the frequency response of the filters via application of DC voltage in the range of -60V to 60V using a bias-tee. Fig. 6 demonstrates the measured frequency response of a wideband acoustically coupled filter across different DC bias voltages, highlighting a large bandwidth tunability of ~15 MHz (~15%).

Prior to application of any DC bias voltage (V_{DC}= 0V), a BW_{-3dB} of 107 MHz is measured. However, application of V_{DC}= 60V and V_{DC}= -60V resulted the tuning of BW_{-3dB} to 117 MHz, and 102.5 MHz, respectively. Such a large BW_{-3dB} variation can be attributed to the local tuning of the dielectric constants in $Al_{0.7}Sc_{0.3}N$ and strong electromechanical coupling by DC fields through the electrostrictive effect arising as a result of the ferroelectric effect in these films.

Finally, the temperature sensitivity of the filter center frequency (i.e. f_0) is measured across the temperature range of 40 - 100°C. Fig. 7 shows the temperature characteristic, highlighting a TCF of -27.74 ppm/°C.

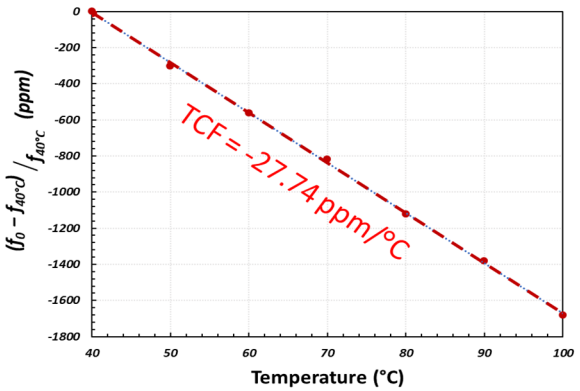

Fig. 7: The measured temperature coefficient of frequency (TCF) of the acoustically coupled filter across 40-100°C temperature range.

CONCLUSION

This paper demonstrates monolithic filters realized from acoustic coupling of various Lamb modes in $Al_{0.7}Sc_{0.3}N$ film. These filters enable realization of wideband filters in small footprints and provide a bandwidth that is configurable through lithographical definition of the IDTs. The filter operation concept is presented and the importance of large electromechanical coupling of $Al_{0.7}Sc_{0.3}N$ to realize large bandwidth is explored using COMSOL simulations. Proof-of-concept filters are fabricated in 1µm $Al_{0.7}Sc_{0.3}N$ film at 2.3 GHz, showing large -3db bandwidths ranging over 70-117 MHz. A large bandwidth tuning of ~15% is demonstrated by exploring the recently discovered ferroelectric properties in $Al_{0.7}Sc_{0.3}N$. This demonstration highlights the promising potential of acoustically coupled $Al_{1-x}Sc_xN$ filter technology for realization of tunable spectral processors for reconfigurable wireless communication systems.

ACKNOWLEDGMENTS

The authors thank the staff at Nanoscale Research Facility at the University of Florida for their help with the device fabrication and Nicholas Rudawski for help with TEM.

REFERENCES

[1] Lakin, K. M. (2002, October). Coupled resonator filters. In *2002 IEEE Ultrasonics Symposium, 2002. Proceedings.* (Vol. 1, pp. 901-908). IEEE.

[2] Abdolvand, R., & Ayazi, F. (2007, June). Monolithic thin-film piezoelectric-on-substrate filters. In *2007 IEEE/MTT-S International Microwave Symposium* (pp. 509-512). IEEE.

[3] Pensala, T., Makkonen, T., Dekker, J., & Ylilammi, M. (2018, October). Laterally Acoustically Coupled BAW Filters at 3.6 GHz. In *2018 IEEE International Ultrasonics Symposium (IUS)* (pp. 1-4). IEEE.

[4] Pan, W., Thakar, V. A., Rais-Zadeh, M., & Ayazi, F. (2012). Acoustically coupled thickness-mode AIN-on-Si band-pass filters-part I: principle and devices. *IEEE transactions on ultrasonics, ferroelectrics, and frequency control*, *59*(10), 2262-2269.

[5] Ghatge, M., Felmetsger, V., & Tabrizian, R. (2018, May). High $k_t^2 \cdot Q$ Waveguide-Based ScAlN-on-Si UHF and SHF Resonators. In *2018 IEEE International Frequency Control Symposium (IFCS)* (pp. 1-4). IEEE.

[6] Fichtner, S., Wolff, N., Lofink, F., Kienle, L., & Wagner, B. (2019). AlScN: A III-V semiconductor based ferroelectric. *Journal of Applied Physics*, *125*(11), 114103.

CONTACT

S. Rassay, tel: +1-321-616-1298; sushantrassay@ufl.edu